Quantitative Electrochemical DNA Microarray on a Monolith Electrode with 10 Attomolar Sensitivity, 100% Specificity, and Zero Background

Shobana Raghunath,[1] Abhijeet Prasad,[2,1] Rahul Tevatia,[2] Jillian.R. Gunther,[3] Santanu Roy,[1] Sunil Krishnan,[3] Ravi F. Saraf[2,*]

[1]Vajra Instruments, Inc, Lincoln, NE 68512; [2]Chemical Engineering, University of Nebraska, Lincoln, NE 68588; [3]MD Anderson Cancer Research Center, Houston, TX 77030; *rsaraf2@unl.edu

Published in *Chemelectrochem* **2018**, 5 (3), 429-433

The manuscript below may be slightly different from the published MS.

Accepted: ChemElectroChem, Nov 2017

Quantitative Electrochemical DNA Microarray on a Monolith Electrode with 10 Attomolar Sensitivity, 100% Specificity, and Zero Background

Shobana Raghunath,[1] Abhijeet Prasad,[2,1] Rahul Tevatia,[2] Jillian.R. Gunther,[3] Santanu Roy,[1] Sunil Krishnan,[3] Ravi F. Saraf[2,*]

[1]Vajra Instruments, Inc, Lincoln, NE 68512; [2]Chemical Engineering, University of Nebraska, Lincoln, NE 68588; [3]MD Anderson Cancer Research Center, Houston, TX 77030; *rsaraf2@unl.edu

Academic titles (in order as they appear): Senior Scientist; Engineer; Senior scientist; Assistant Professor; Senior Scientist; Professor; Professor.

Abstract

Circulating microRNA are promising diagnostic and prognostic biomarkers of disease in quantitative blood tests. A label-free, PCR-free, electrochemical microarray technology on a monolith electrode is described, with 10 attomolar (aM) sensitivity and responsiveness to binding of < 1 zeptomole targets to immobilized ssDNA probes with zero background. Specificity is 100% in a mixture with five nonspecific miRNA each with a 10^3-fold higher concentration. Direct measurement on plasma-derived miRNA without cDNA conversion and PCR demonstrated multiplexing and near ideal quantitative correlation with an equivalent pure sample. The dynamic range is a target concentration ranging from 10^{-2} to 10^3 femtomolar (fM). This PCR-free novel technology can be applied as a test for cancer diagnosis/prognosis to detect 10^3 copies of a miRNA sequence in RNA extracted from 100 µL of plasma.

Keywords: microarray • DNA sequencing • microRNA • cancer diagnosis • blood test • electrochemical analysis

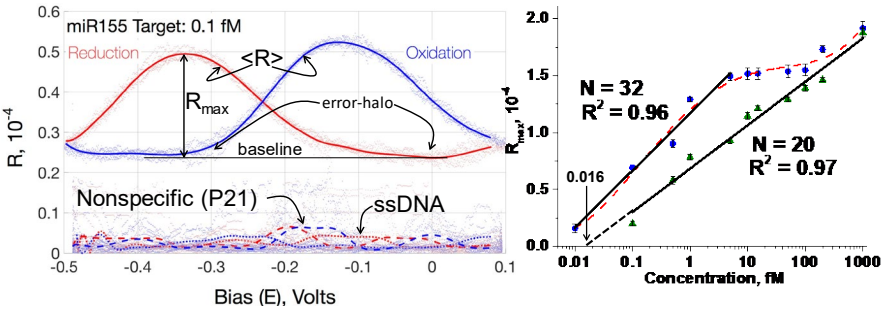

TOC Figure: A DNA chip technology is developed to measure binding to microarray on a monolith electrode by probing local redox on each spot. The redox peak, R_{max}, was zero for no-binding (ssDNA) and non-specific binding. The binding is enhanced electrochemically in <30 mins to attain dynamic range of 10^{-2} to 10^3 femtomolar. The method is applied to measure microRNA extracted from plasma with no PCR and cDNA conversion.

Accepted: ChemElectroChem, Nov 2017

Cell-derived circulating microRNA (miRNA) in blood, urine, and saliva could be utilized to develop a blood test for the diagnosis of diseases and for personalized therapy. It was recently discovered that most circulating miRNAs in blood are cell free and are remarkably stable in body fluids because of complexation with argonaute proteins,[1] making them attractive for screening and early detection of diseases, particularly cancer.[2;3] MiRNAs are noncoding ~22 nucleotide (nt) long, single-stranded RNA (ssRNA) sequences that bind to mRNA by their 5'-seed region (2-8 nt long) to negatively regulate mRNA expression.[4] MiRNAs regulate ~60% of genes involved in a range of cellular activities, such as cell cycle, proliferation, differentiation, metabolism, inflammation, and immune response.[5;6] As one miRNA can regulate multiple mRNAs and multiple miRNAs can regulate a single mRNA,[7] a panel of miRNA is required to diagnose cancer at high specificity.[8] Meta-analyses for a variety of cancers, for example, colorectal,[9] lung,[10] and pancreatic[11] cancer, suggest that profiling dysregulation of several miRNA sequences can lead to diagnosis at over 85% sensitivity and specificity. Thus, the challenge in developing a screening test is to quantitatively profile a panel of miRNA sequences with proper controls [12] at a sensitivity of ~10 copies in RNA extracted from a µL of blood [13] over a dynamic range of five orders. [14]

The small size of miRNAs (unfortunately) leads to large variations in melting temperature due to small differences in sequence, making it difficult to multiplex a large number of sequences using qPCR, the gold standard.[15] Furthermore, synthesis of cDNA from miRNA by reverse transcriptase (RT) requires ~ 10^5 copies for efficient conversion.[16;17] Hence, RNA from ~10 mL of plasma is required to detect 10 copies in extracted RNA. To avoid PCR, several approaches have been developed to obtain a limit of detection (LOD) in the fM to aM range: the nanopore translocation method,[18] an electrochemical transistor made from nanowires,[19] surface plasmon resonance in nanoprisms,[20] and differential pulse voltammetry from nanoelectrodes,[21] which have reported LODs of 100 fM, 1 fM, ~ 40 aM, and 100 aM, respectively. A chip with a nanoelectrode array has been shown to directly measure multiple miRNA sequences from plasma without the cDNA conversion and PCR.[22] The analysis is usually nonabsolute, requiring a difference in signals before and after the binding between the probe and the target miRNA,[19-22] which may amplify error. Individual drops on each microspot need to be placed to confine the diffusion length,[19;21;22] which may limit the device density and result in possible error due to solvent evaporation.

In this study, an electrochemical microarray patterned on a monolith electrode was developed resulting in robust statistics. To gain high sensitivity, a method was developed to focus ~1,800 molecules to microarray spots from ~0.3 mL solution and measure <1 zeptomole target-to-probe binding. The combination allowed the technology to obtain sensitivity of 10 attomolar (i.e., ~0.15 fg/µL) with 100% specificity over a dynamic range of five orders of magnitude. The unique feature not shown before is absolute signal with zero background, i.e., the signal for no binding is zero (which was confirmed for every chip).

For the study, using a 1.2 by 1.2 cm chip with five longer and two shorter (control) electrodes, an array of seven and three 50-µm holes (i.e., spots) were patterned on a photoresist, respectively, using photolithography (**Fig. 1(a)**, and **Supporting Information (SI), Sections S.1 and S.2, for details**). Single-stranded DNA (ssDNA) probes with thio-

terminated sequences were immobilized on the spots of an exposed Au electrode (**SI, Section S.3**). The binding was performed in a solution of target molecules in 100 mM of phosphate buffer (PB) with 50 mM of auxiliary ion $[Fe(CN)_6]^{4-}$ by cyclic voltammetry (CV) (**Fig. 1(b)**). The CV ramp potential (V) applied between the working electrode (WE) and the reference electrode (RE) was from -0.4 to 0.3 V at a ramp rate of 50 mV/s. The amount of binding on each of the five electrodes was controlled by the number of cycles, N. Importantly, although the electric-field-influenced binding has been demonstrated before,[23] the novelty here is the significant enhancement in binding due to the inclusion of redox ion, $[Fe(CN)_6]^{4-}$. As the positive potential attracts the negatively charged target molecules, beyond +220 mV, $[Fe(CN)_6]^{4-}$ oxidizes to $[Fe(CN)_6]^{3-}$ causing the EDL to discharge to enhance the electric field penetration from 10^2 nm (at no redox) to typically 10^0 μm (during redox reaction).[24;25] The deeper penetration of the electric field is independently shown by differential interferometry where the ion oscillation was significantly enhanced, leading to a peak at V close to redox.[25;26] The binding process is called electrochemical redox enhanced binding (EREB). The effect of $[Fe(CN)_6]^{4-}$ on binding efficiency is discussed later. Subsequent to vigorous washing, the uncovered area of the electrode was coated with a monolayer of mercaptohexanol (MCH) at 37 °C (**SI, Sections S.1 and S.4**).

Binding of targets to an array of probes on a monolith electrode was measured electrochemically by scanning a laser. It is known that methylene blue (MB) undergoes redox by specifically binding to the probe-target duplex by electron transport through π-π stacked base pairs.[27] A differential reflectometer was designed and developed to measure local redox of MB on each microarray spot on the electrode (**Fig. 1(c)**). Reflectivity measurements were performed in 100 mM of PB containing 10 μM of MB and 50 mM of $[Fe(CN)_6]^{4-}$. The latter is the mediator for MB redox.[27] The reflectivity was performed during CV with a potential (E) from -0.5 to 0.1 V to cover the redox of MB (at ~-0.2 V). To measure differential reflectivity, a periodic AC potential of frequency, ω = 2 KHz, and an amplitude of 100 mV was added to the CV ramp. The detector measured a DC signal corresponding to incident intensity, R_O, and an AC signal at ω due to oscillation in the reflected light intensity caused by the oscillation of the ions due to the AC potential at ω (see **SI, Section S.5** for the mechanism). The amplitude of the AC signal, R_A, was obtained from the lock-in amplifier tuned to ω to measure differential reflectivity, $R = R_A/R_O$, as low as 0.001%.

Typical raw data on a spot with ssDNA probe, P155, that specifically binds to target T155 (ssDNA equivalent of miR155), showed oxidation and reduction peaks for MB (**Fig. 1(d)**). The peaks were because the ion oscillation was maximum for E at maximum redox currents owing to deeper penetration of the electric field into the solution caused by discharge of the EDL.[25;26] As R corresponds to charge at the interface, the reflectometer is called a scanning electrometer for electrical double layer (SEED). Superposing the various cycles of R(t) and filtering the high frequency noise, the average reflectivity, <R>(E), was obtained from ~20 cycles (**Fig. 1(e) and Fig. S5 in SI**). The small error halo indicated that the oscillation of R was highly periodic leading to statistically robust R_{max}. As the signal is a reduction of MB, R_{max} is defined with respect to the reduction peak. The signal has a baseline because of ubiquitous oscillation of the ions due to AC potential at 2 KHz at all potentials, E, related to the optical properties of the solution (see **SI, Equation (4)**). All subsequent data presented is after baseline subtraction on the reduction peak.

Importantly, on the same electrode, the spot with a nonspecific probe (i.e., P21) showed no MB redox peak. Thus, the specificity from differential reflectivity was 100%. The specificity was confirmed for each electrode on the chip. Specificity in a more aggressive environment is described in Fig. 3.

The control electrode incorporated in every chip is an important unique feature of this method. No potential was applied during EREB on the shorter control electrodes. Each control electrode had a blank (i.e., bare Au) spot and one spot each with immobilized P155 and P21. All spots were covered with an MCH monolayer after EREB. For good quality data, all of the six spots on the two control electrodes should show no redox. A signal on the blank spot indicates poor MCH filling which would lead to poor specificity where the signal could erroneously estimate target copies by as high as 3-fold (**SI, Section S.6**). Importantly, the spots with P155 and P21 probes on the control electrode should show no redox indicating that the signal is zero, if no binding occurs (i.e., ssDNA in **Fig. 1(e)**). Thus, the R_{max} reported will be an absolute measurement of the amount of specific binding. The absolute nature of the signal ensured for every chip is a unique feature of the method not reported before.

At constant, N, as expected, E versus <R> (at N = 20) showed a monotonic decrease in the overall signal as the concentration decreased from 1 pM to 0.1 fM (**Fig. 2(a)**). By increasing N from 20 to 32 cycles, the binding increased significantly to observe a signal from a target concentration of 0.01 fM (**Fig. 2(a)**). R_{max} at constant N (= 20) increased linearly (at a fitness of 97%) with a target concentration on a logarithmic scale of over four orders of magnitude (**Fig. 2(b)**). Each R_{max} in the calibration curve for N = 20 and 32 (**Fig. 2(b)**) was an average of over 15 points (i.e., three points with a 6 µm laser beam on each of the five 50 µm spots on the electrode). Thus, five target concentrations were measured on each chip. The error bar was the standard deviation. The small error bar indicated excellent uniformity of immobilization, and reproducibility of the measurement. Extrapolation to R_{max} = 0 (**Fig. 2(b)**) indicated that the LOD for N = 20 and 32 was ~16 aM and 3.9 aM, respectively. The practical sensitivity for the study was 10 aM or 0.15 fg/µL. For 0.3 mL solution during EREB, 10 aM corresponded to ~1,800 molecules. Uniform binding of over five array spots, implied that SEED can detect binding of <360 target molecules, i.e., a responsivity of <1 zeptomole.

Using SEED, the nature of the EREB process was characterized. Due to the increase in a larger penetration depth due to oxidation of $[Fe(CN)_6]^{4-}$ noted above, the R_{max} increased from ~0.3×10^{-4} to 1.3×10^{-4} for 1 fM of target due to the addition of 50 mM $[Fe(CN)_6]^{4-}$ during the EREB process at N = 32 cycles (Fig. 2(c)). Based on **Fig. 2(a)**, this remarkable increase in R_{max} by 1×10^{-4} due to inclusion of $[Fe(CN)_6]^{4-}$ was equivalent to an increase in target concentration by tenfold. As the V ramped to negative values, the loosely attached target molecules were repelled to reactivate the probes. The negative potential of V = -0.4 V was sufficient for efficient repulsion of the nonspecific target to obtain the observed 100% specificity.

Three types of samples were studied to evaluate multiplexing and specificity in complex systems. First, a synthetic mixture of miR155 (1fM) and miR21(10 fM) in a background of five miRNA each with a concentration of 1 pM (sequences and more detail shown in **SI, Section S.7**) was analyzed on a chip at different N (**Fig. 3(a)**). The R_{max} for T155 was consistent with values in **Fig. 2(b)**, indicating no interference from the background. The

R_{max} for T21 was higher than for T155 and was also consistent with a higher concentration. Thus, EREB/SEED can quantitatively measure multiple sequences in significantly larger background.

Second, RNA was extracted from 200 µL of plasma from a healthy donor and spiked with *C. elegans* miR39a. After reconstituting the RNA in 300 µL of PB buffer, EREB was carried at 4 ^{O}C to avoid RNA degradation. The R_{max} for miR39a in buffer (i.e., calibration curve) was measured (**Fig. 3(b)**) and compared to R_{max} spiked in plasma for a concentration ranging from 10 aM to 1 pM (**Fig. 3(b), inset**). The correlation was remarkable, showing that the effect of background due to other molecules in plasma is negligible. Because it is possible to measure ~200 copies of target (i.e., 10 aM in 300 µL) extracted from 200 µL of plasma, the method can safely measure ~10^3 copies of (specific) miRNA extracted from 100 µL of plasma at zero background.

Third, to demonstrate multiplexing and quantitative comparison to qPCR, RNA was extracted from the plasma of a colorectal cancer patient (CRC) and a normal donor (ND) and spiked with miR39 of *C. elegans*. The copy number of each miRNA was normalized with respect to R_{mx} for a miR39a spike in the extracted RNA (using the calibration curve for SEED (**Fig. 3(b)**) and the standard qPCR curve (**SI, Fig. S8**)). In all cases, the dysregulation by SEED and qPCR was consistent; and the relative copy numbers were quantitatively comparable (**Fig. 3(c)**). For miR34a, the values were in the opposite direction because the copy number was close to spiked miR39a; however, the magnitudes were comparable (see **SI, Section S.8 and Table**).

In summary, we report a novel technology to electrochemically measure binding on a microarray patterned on a monolith electrode. The sensitivity is 10 aM (i.e., ~0.15 fg/µL) with a limit of detection of ~3.9 aM at 100% specificity and a dynamic range of five orders of magnitude with robust statistics. By spiking plasma with miRNA, a direct analysis from extracted RNA without PCR and cDNA conversion was illustrated with remarkable correlation from 10 aM to 1 pM of spiked miR39a. Multiplexing on a single chip was demonstrated by directly measuring five miRNA plus one negative control for RNA extracted from 200 µL of plasma from a healthy donor and a cancer patient. The comparison to qPCR was quantitative for all of the miRNA targets. This label-free technology could be implemented as a tool for prognostic and diagnostic application.

Acknowledgement: RFS thanks NIH/NCI (CA186788-01; CA199058-01) and Nebraska Department of Economic Development (16-01-171; 15-01-055) for financial support.

Author contributions: Shobana Raghunath conducted the majority of the experiments and data generation; Abhijeet Prasad contributed to instrumentation and data analysis; Rahul Tevatia and Raghunath contributed to plasma experiments; everyone contributed to experimental design, data interpretation, and manuscript preparation.

Supporting Information: Details on the overall method, experimental condition, and chip fabrication, mathematical derivation of reflectivity modulation, and the effect of different fabrication conditions, such as MCH coverage, are discussed.

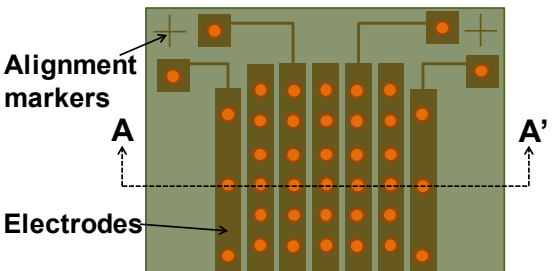

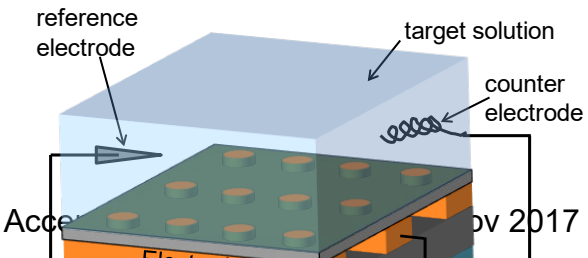

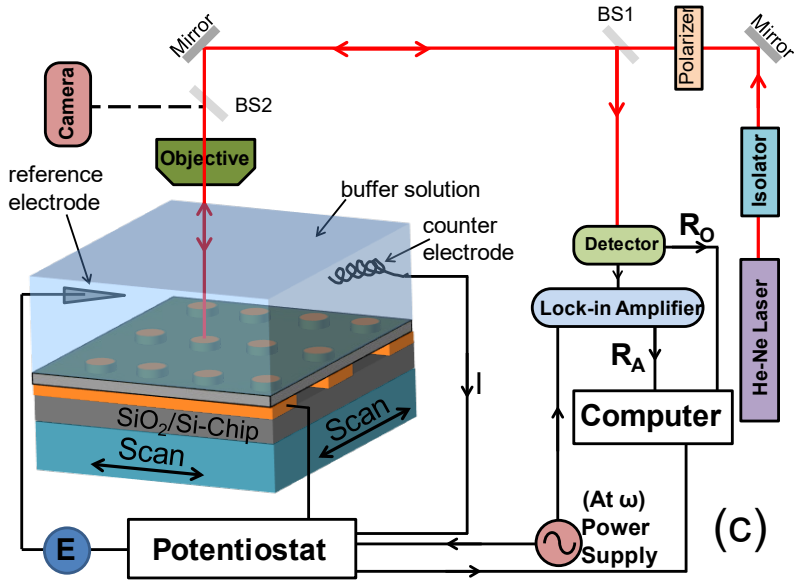
Mirror
BS1
Polarizer
Mirror
Camera
BS2
Objective
reference electrode
buffer solution
counter electrode
Detector
R_O
Isolator
Lock-in Amplifier
R_A
He-Ne Laser
I
SiO_2/Si-Chip
Scan
Scan
Computer
(At ω) Power Supply
E
Potentiostat
(c)

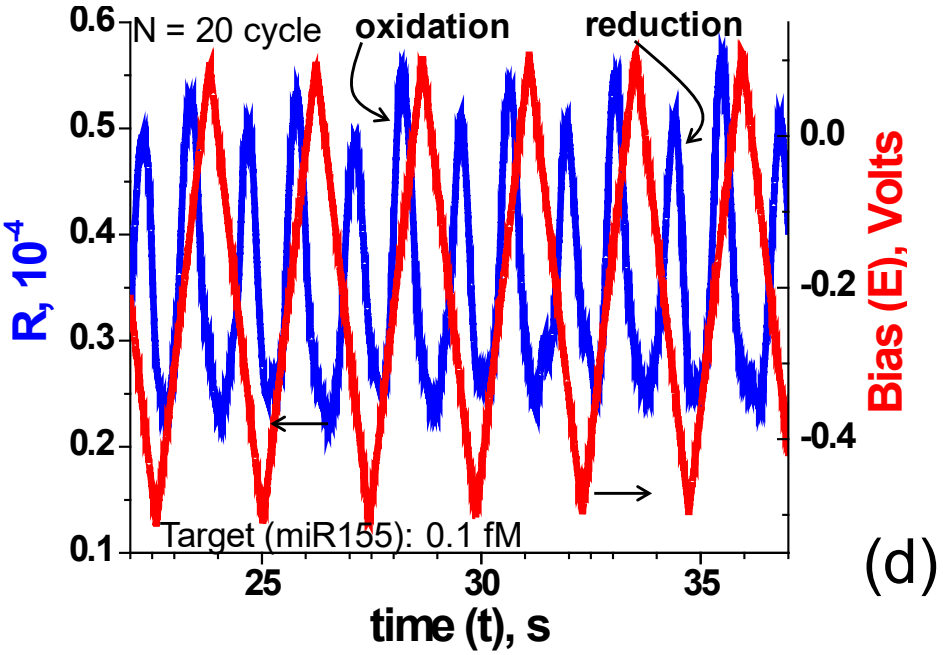
N = 20 cycle
oxidation
reduction
R, 10^{-4}
Bias (E), Volts
0.6
0.5
0.4
0.3
0.2
0.1
0.0
-0.2
-0.4
Target (miR155): 0.1 fM
25
30
35
time (t), s
(d)

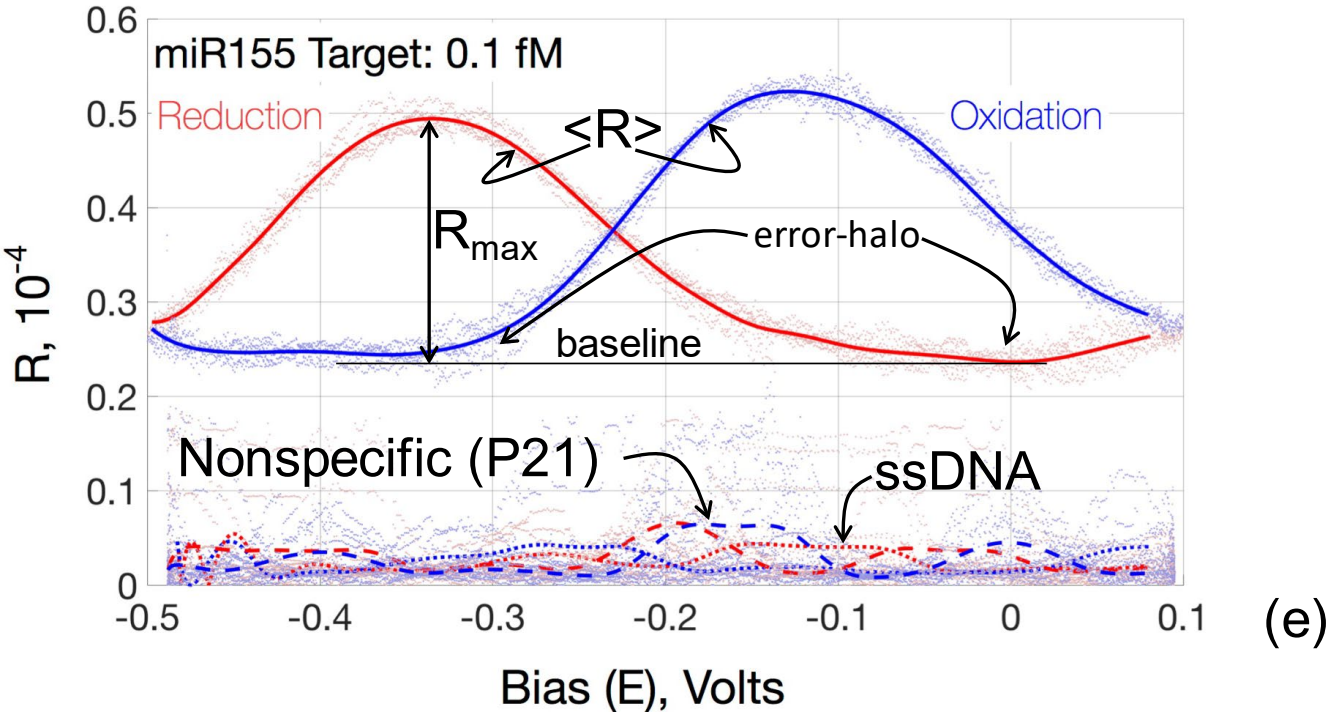

Figure 1: (a) The electrodes and circuitry are on a ~ 200 nm thick SiO_2 layer on Si. The etched photoresist (SU8) exposes the underlying electrode (cross-section A-A', not to scale). The shorter electrodes are controls where no EREB potential is applied. (b) The EREB setup is a three-electrode system controlled by a potentiostat (AutoLab PGSTAT302N). The RE and CE are Ag/AgCl and Pt wire, respectively. A potential, V, is applied between the chip electrode (WE) and RE; and current, I, is measured between WE and CE. (c) The differential reflectivity is measured during CV. As the potential, E, is ramped between WE and RE, the modulation in reflected light intensity, R_A, at ω is amplified by the lock-in amplifier. The incident light intensity, R_O, is measured as a DC signal. (d) Raw data: R and E as a function of time, t (for specific binding). Full scan is in SI, Fig.S5. (e) E versus R with "error halo" corresponds to cycle-to-cycle variations. The ssDNA is R from a spot with P155 on the control electrode not subjected to EREB. The nonspecific spot corresponds to the spot with P21 on the same electrode as the specific spots. R_{max} is defined for the reduction peak with respect to the baseline.

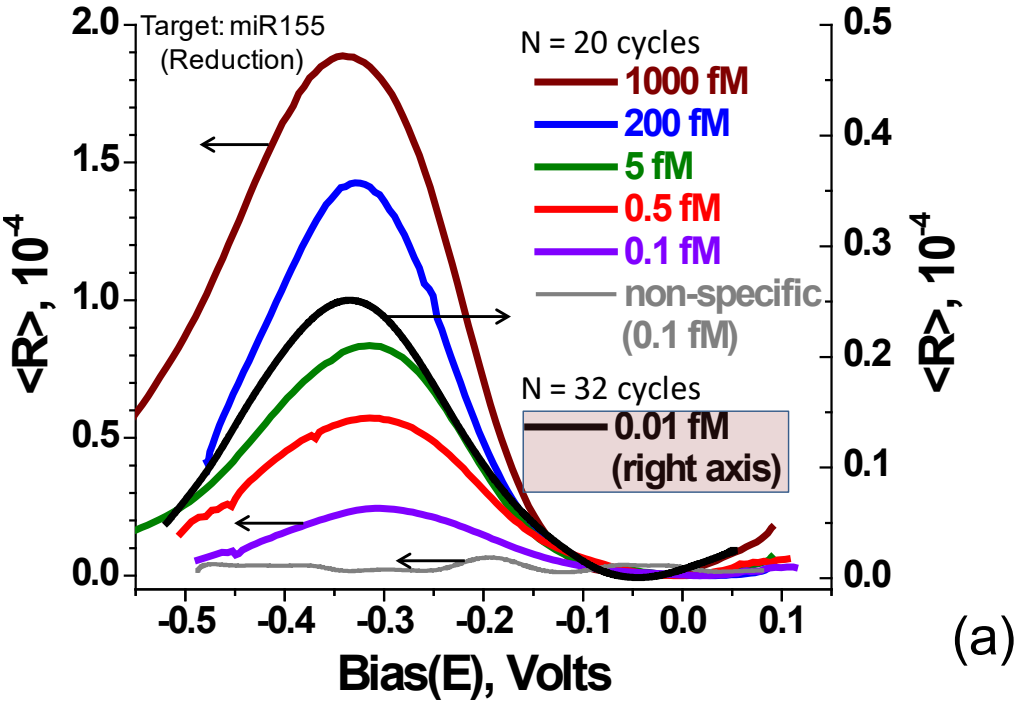
Target: miR155
(Reduction)
N = 20 cycles
1000 fM
200 fM
5 fM
0.5 fM
0.1 fM
non-specific
(0.1 fM)
N = 32 cycles
0.01 fM
(right axis)
<R>, 10^-4
<R>, 10^-4
Bias(E), Volts
(a)

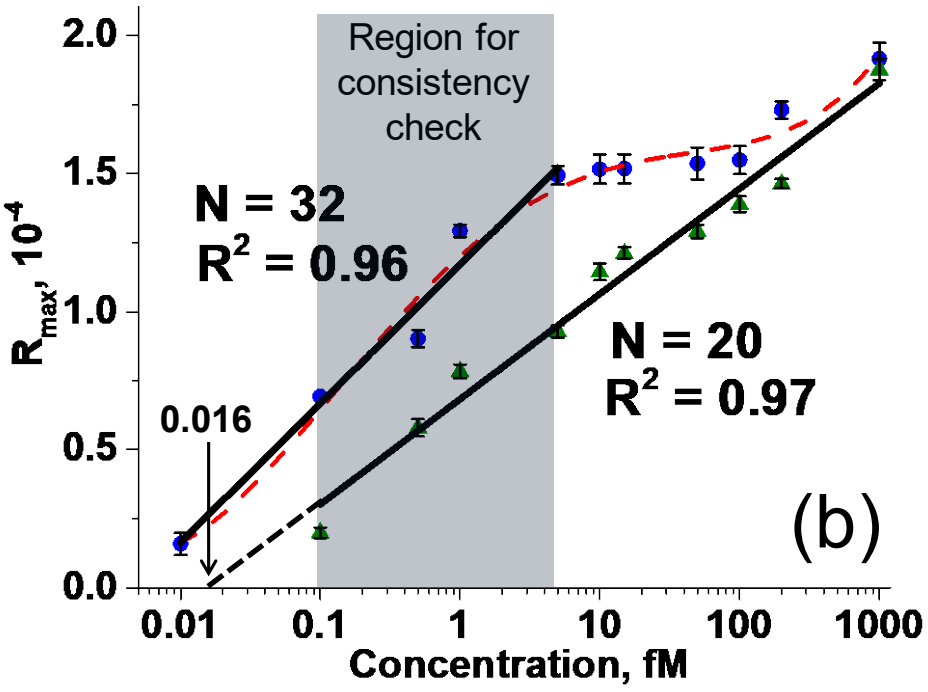
Region for
consistency
check
N = 32
R^2 = 0.96
N = 20
R^2 = 0.97
0.016
R_max, 10^-4
Concentration, fM
(b)

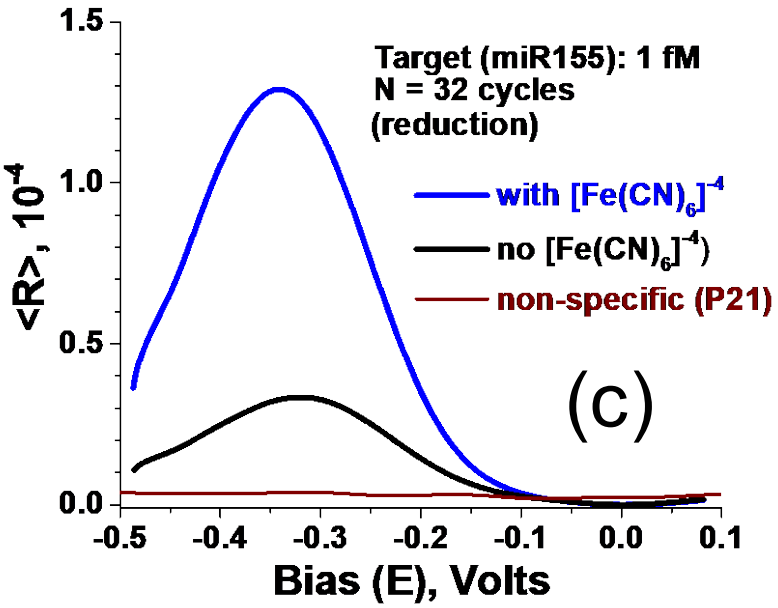

Figure 2: (a) Typical baseline corrected E versus <R> for various miR155 target concentrations on the spot with P155 for EREB performed at N = 20. The LOD was 0.01 fM at N = 32 (right axis). (b) R_{max} as a function of target concentration. Each data point was averaged over 15 E versus <R> scans. All of the controls and the nonspecific spot had zero signals. (c) Effect of auxiliary ions on reflectivity was measured on the same spot without removing the chip from the sample chamber. First the experiment with no $[Fe(CN)_6]^{4-}$ (in PB buffer) was conducted, followed by a vigorous wash with distill water before the second experiment containing $[Fe(CN)_6]^{4-}$ in PB buffer.

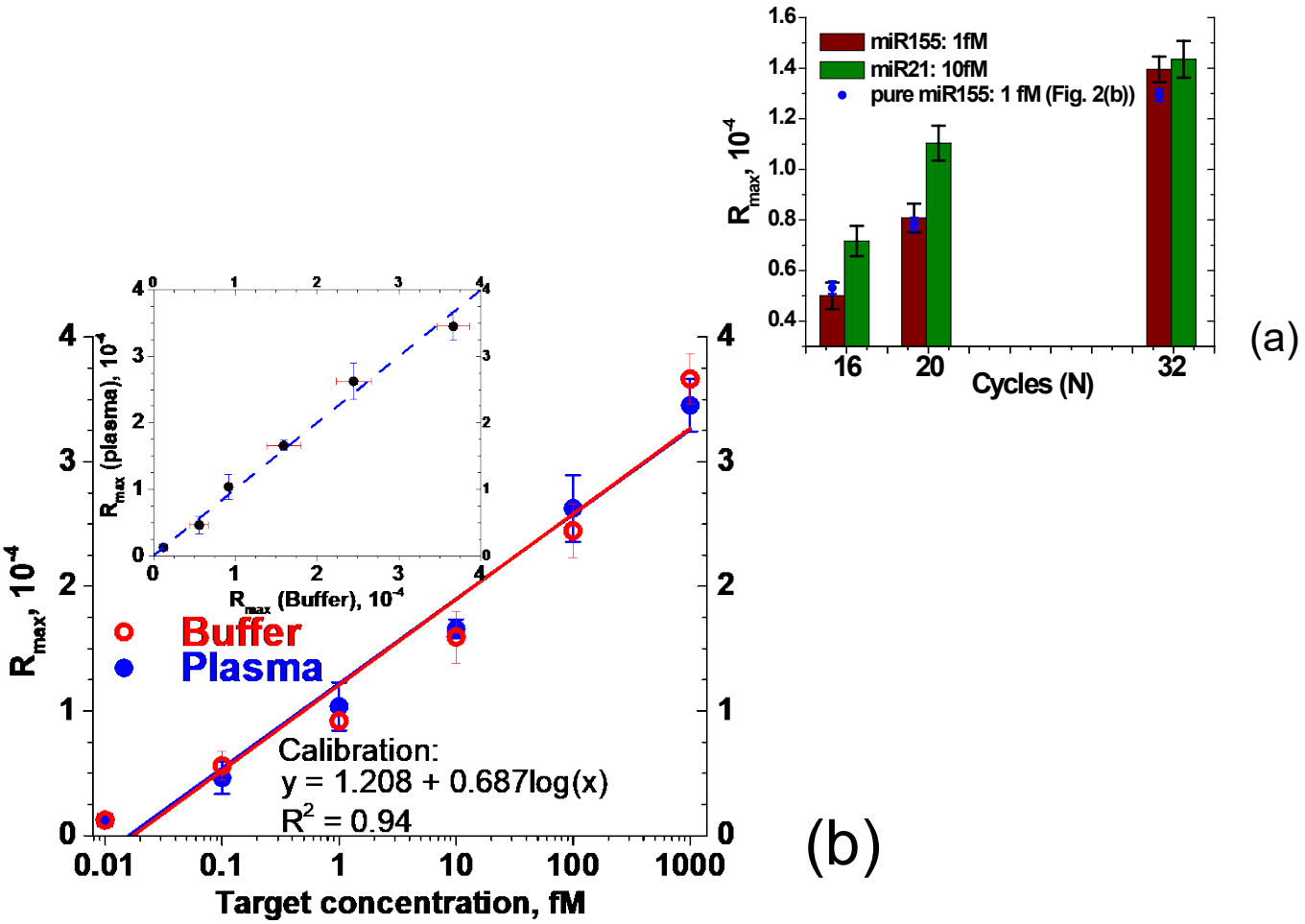

Figure 3: (a) The R_{max} on a chip for specific binding of miR155 and miR21 with five background miRNA each at 1 pM concentration. (b) Comparison of R_{max} for miR39a in standard EREB buffer (buffer) and spiked in extracted RNA from plasma and reconstituted in identical buffer (plasma). Inset: Comparison of signal from pure and plasma samples with a miR39a concentration ranging from 0.01 to 10^3 fM. (c) Comparison of patient and healthy plasma for four miRNA by qPCR and SEED (on a single chip).

References

[1.] A. Turchinovich, L. Weiz, A. Langheinz, B. Burwinkel, *Nucleic Acids Research* **2011,** *39* 7223-7233.

[2.] S. P. Nana-Sinkam, C. M. Croce, *Clinical Pharmacology & Therapeutics* **2013,** *93* 98-104.

[3.] G. Reid, M. B. Kirschner, N. van Zandwijk, *Critical Reviews in Oncology Hematology* **2011,** *80* 193-208.

[4.] D. P. Bartel, *Cell* **2009,** *136* 215-233.

[5.] J. Ahmad, S. E. Hasnain, M. A. Siddiqui, M. Ahamed, J. Musarrat, A. A. Al-Khedhairy, *Indian Journal of Medical Research* **2013,** *137* 680-694.

[6.] G. Di Leva, M. Garofalo, C. M. Croce, *MicroRNAs in Cancer*, **2014,** pp. 287-314.

[7.] B. P. Lewis, I. H. Shih, M. W. Jones-Rhoades, D. P. Bartel, C. B. Burge, *Cell* **2003,** *115* 787-798.

[8.] H. Y. Lan, H. Q. Lu, X. Wang, H. C. Jin, *Biomed Research International* **2015**.

[9.] Z. Kanaan, H. Roberts, M. R. Eichenberger, A. Billeter, G. Ocheretner, J. M. Pan, S. N. Rai, J. Jorden, A. Williford, S. Galandiuk, *Annals of Surgery* **2013,** *258* 400-408.

[10.] U. Vosa, T. Vooder, R. Kolde, J. Vilo, A. Metspalu, T. Annilo, *International Journal of Cancer* **2013,** *132* 2884-2893.

[11.] Z. L. Pei, S. M. Liu, J. T. Huang, X. Zhang, D. Yan, Q. L. Xia, C. X. Ji, W. P. Chen, X. Y. Zhang, J. Q. Xu, J. Wang, *Oncotarget* **2017,** *8* 22616-22624.

[12.] C. C. Pritchard, E. Kroh, B. Wood, J. D. Arroyo, K. J. Dougherty, M. M. Miyaji, J. F. Tait, M. Tewari, *Cancer Prevention Research* **2012,** *5* 492-497.

[13.] P. S. Mitchell, R. K. Parkin, E. M. Kroh, B. R. Fritz, S. K. Wyman, E. L. Pogosova-Agadjanyan, A. Peterson, J. Noteboom, K. C. O'Briant, A. Allen, D. W. Lin, N. Urban, C. W. Drescher, B. S. Knudsen, D. L. Stirewalt, R. Gentleman, R. L. Vessella, P. S. Nelson, D. B. Martin, M. Tewari, *Proceedings of the National Academy of Sciences of the United States of America* **2008,** *105* 10513-10518.

[14.] R. M. Graybill, R. C. Bailey, *Analytical Chemistry* **2016,** *88* 431-450.

[15.] I. H. Lee, S. S. Ajay, H. M. Chen, A. Maruyama, N. L. Wang, M. G. McInnis, B. D. Athey, *Nucleic Acids Research* **2008,** *36* .

[16.] J. A. Miranda, G. F. Steward, *Journal of Virological Methods* **2017,** *241* 1-10.

[17.] Q. Zhao, S. Q. Deng, G. X. Wang, C. C. Liu, L. Y. Meng, S. S. Qiao, L. Shen, Y. Zhang, J. H. Lu, W. S. Li, Y. Z. Zhang, M. Wang, R. G. Pestell, C. L. Liang, Z. R. Yu, *Oncotarget* **2016,** *7* 21865-21874.

[18.] Y. Wang, D. L. Zheng, Q. L. Tan, M. X. Wang, L. Q. Gu, *Nature Nanotechnology* **2011,** *6* 668-674.

[19.] G. J. Zhang, J. H. Chua, R. E. Chee, A. Agarwal, S. M. Wong, *Biosensors & Bioelectronics* **2009,** *24* 2504-2508.

[20.] G. K. Joshi, S. itz-McElyea, T. Liyanage, K. Lawrence, S. Mali, R. Sardar, M. Korc, *Acs Nano* **2015,** *9* 11075-11089.

[21.] H. Yang, A. Hui, G. Pampalakis, L. Soleymani, F. F. Liu, E. H. Sargent, S. O. Kelley, *Angewandte Chemie-International Edition* **2009,** *48* 8461-8464.

[22.] J. Das, I. Ivanov, L. Montermini, J. Rak, E. H. Sargent, S. O. Kelley, *Nature Chemistry* **2015,** *7* 569-575.

[23.] I. Y. Wong, N. A. Melosh, *Nano Letters* **2009,** *9* 3521-3526.

[24.] A. J. Bard, L. R. Faulkner, *Electrochemical Methods: fundamentals and Applications*, 2nd ed. J. Wiley & Sons, New York, **2001**.

[25.] S. W. Lee, J. Lopez, R. F. Saraf, *Electroanalysis* **2013,** *25* 1557-1566.

[26.] S. W. Lee, J. Lopez, R. F. Saraf, *Biosensors & Bioelectronics* **2013,** *47* 408-414.

[27.] T. G. Drummond, M. G. Hill, J. K. Barton, *Nature Biotechnology* **2003,** *21* 1192-1199.

446 **Supporting Information (SI)**

447 **PCR-Free, Label-Free Quantitative Electrochemical Microarray**
448 **on a Monolith Electrode**

449 Shobana. Raghunath,[1] Abhijeet Prasad,[2,1] R. Tevatia,[2] Jillian.R. Gunther,[3] S. Roy,[1]
450 Sunil Krishnan,[3] R.F. Saraf[2,*]

451 [1]Vajra Instruments, Inc, Lincoln, NE 68512; [2]Chemical Engineering, University of
452 Nebraska, Lincoln, NE 68588; [3]MD Anderson Cancer Research Center, Houston, TX
453 77030 *rsaraf2@unl.edu

454

455

456 **S.1 Overall summary of all the steps used in the technology**

457 Further details on various steps described are in the various sections below.

458 **Chip Fabrication:** The microarray was made on a 1.2 by 1.2 cm Si chip with Au
459 electrodes and accompanying circuitry for power and signal on ~200 nm SiO_2 to provide
460 an insulating surface. (Fig. 1(a)). The chip was cleaned in acetone, water, and ethanol
461 followed by O_2 plasma and subsequently immersed in piranha solution for ~60 sec. The
462 chip was dried by blowing clean N_2 from a 0.2 µm filter. Photoresist SU8 (Microchem
463 2025) was diluted by adding three times the volume of cyclopentanone which was spin
464 cast on the chip at 3,000 rpm for 60 sec. to produce an ~ 500-nm thick film. The chip was
465 prebaked for 45 sec. at 80 °C. The film was exposed to Xe light (300 W) for 45 sec.
466 through a contact mask with a Cr metalized pattern on quartz. The chip was post-baked
467 for 45 sec. at 80 °C and developed in Microchem SU8 developer. The chip was then
468 washed with water/isopropanol for ~ 60 sec and hard baked at 140 °C for 2 hr. The
469 resulting pattern on each electrode was a microarray of 50 µm holes exposing the
470 underlying Au electrode.

471 **Probe Immobilization:** The immobilization on the spots was obtained by locally
472 dispensing 5 µM solution of the probe in 1 M of phosphate buffer (PB) using an Arrayit®
473 capillary pin with tip of ~20 µm (Fig. S2). The 5 nL solution dispensed on each spot was
474 held by surface tension (Fig. S3). Each spot of the chip was exposed to the probe solution
475 drop at 19 °C in a humidified chamber to avoid evaporation during the immobilization
476 process for at least 16 hrs. The actual exposure was for only 2 hrs. The chip was washed
477 and the process repeated again to obtain higher immobilization density. All of the
478 solutions and the washing were performed using RNAse-free water (Invitrogen).

479 **Electrochemical Redox-Enhanced Binding (EREB) Process:** Subsequent to vigorous
480 washing, EREB was performed in a (10 aM to 1 pM) solution of target molecules in 100
481 mM of phosphate buffer (PB) with 50 mM of auxiliary ion $[Fe(CN)_6]^{4-}$ by cyclic voltammetry
482 (CV). The CV ramp potential (V) applied between the working electrode (WE) and the
483 reference electrode (RE) was from -0.4 to 0.3 V at a ramp rate of 50mV/s. As the positive

potential attracts the negatively charged target molecules, beyond +220 mV, $[Fe(CN)_6]^{4-}$ oxidizes to $[Fe(CN)_6]^{3-}$ causing the EDL to discharge to enhance the electric field penetration from 10^2 nm (at no redox) to typically 10^0 μm (during redox reaction).[1,2] To note is that the electric-field-influenced binding has been demonstrated before.[3] The novelty in this method is the significant enhancement in binding due to the inclusion of redox ion. The scanning range of EREB was optimized using SEED.

MCH Filling Process: The MCH coating was one of the critical aspects of the fabrication. The goal was to completely coat all of the exposed Au electrode surfaces after the the target binding step such that there was no signal on all of the three spots of the control electrode: the blank spot and the two spots with (immobilized) P155 and P21. The control electrode was not subjected to EREB, thus the spots had no binding. A signal on the control electrode would imply that the quality of MCH is poor and the signal on the active electrodes (that were subjected to EREB) is not absolute.

The MCH immobilization was performed in two steps. The chip was exposed to vapors from a 0.5 mL solution of 10 mM MCH in RNAse-free water (Invitrogen) at 37 °C for 10 hr. The process is called atomic layer deposition (ALD). The chip was dry with no condensation of water during ALD. After rinsing in autoclaved DI water, the chip was then immersed in a 1 mL solution of 10 mM MCH in 30% HPLC grade ethanol for 3 hours with vigorous shaking at 100 rpm in an incubator at 37 °C. The chip was subsequently rinsed and immersed in solution for differential reflectivity measurement. All of the solutions and washing /rinsing was performed in RNAse-free water (Invitrogen). MCH filling is after the EREB process to obtain good binding.

Differential Reflectivity Measurements (Scanning Electrometer for Electrical Double-layer (SEED)): Differential reflectivity was performed during CV with a potential (E) from -0.5 to 0.1 V to cover the redox of MB (at ~ -0.2 V). A periodic AC potential of frequency, ω = 2 kHz, and amplitude of 100 mV were added to the CV ramp. The detector measured a DC signal corresponding to incident intensity, R_O, and an AC signal at ω due to oscillation in the reflected light intensity caused by the oscillation of the ions due to the AC potential at ω. The amplitude of the AC signal, R_A, was obtained from the lock-in amplifier tuned to ω to measure differential reflectivity, $R = R_A/R_O$, as low as 0.001%. The peaks were observed in Fig. 1(e) because the ion oscillation was maximum for E at maximum redox currents owing to deeper penetration of the electric field into the solution.[4]

qPCR Analysis: Total RNA was extracted using a standard kit (RNeasy Plus kit from QIAGEN). The total RNA was converted to cDNA using First Strand Synthesis kit (Clontech Lab., Inc). SYBR™ Green method (Clontech Lab., Inc) was adopted to perform the cDNA synthesis and qPCR measurements on the qPCR machine (QuantStudio™ 3 RT-PCR, ABI, USA). Briefly, 3.75 μL of a standard solution with known concentration was added to reverse transcriptase buffer and enzyme (the final reaction volume was 10 μL).

The reaction was allowed to incubate at 37 ^{O}C for one hour, followed by denaturation of the RT enzyme at 85 ^{O}C for five minutes. The synthesized cDNA was diluted by 10-fold. A 0.8 µL portion was added to the master stock (SYBR Advantage Premix, ROX, miRNA-specific 5' and 3' primers) resulting in the final volume of 10 µL. Melting curves on qPCR products were also generated to confirm specificity of the amplification. After qPCR, the data was analyzed while setting the threshold fluorescence to 0.059 arbitrary units. The threshold was set to a constant for biological replicates. Based on Ct values, the relative fold change in targeted miRNAs was calculated. Quantification of miRNA copy number was calculated from standard curve. For the standard curve, at least 10^6 copies are needed in the RT mix, consistent with the literature (see Fig. S9 in Section S.9).[5]

S.2 Chip Fabrication

The microarray was made on a 1.2 by 1.2 cm Si chip with Au electrodes and accompanying circuitry for power and signal (Fig. 1(a)). The chip is passivated with ~200 nm SiO_2 to provide an insulating surface. The chip was coated with SU8 photoresist to make seven and three 50-µm holes on the longer and shorter electrodes, respectively, using a standard photolithography process (Fig. S1). Briefly, the chip was cleaned in acetone, water, and ethanol followed by O_2 plasma and subsequently immersed in piranha solution for ~60 sec. The piranha solution was freshly prepared by mixing H_2SO_4 in H_2O_2 at a volume ratio of 3:1, respectively. The chip was dried by blowing clean N_2 from a 0.2 µm filter. Photoresist SU8 (Microchem 2025) was diluted by adding three times the volume of cyclopentanone which was spin cast on the chip at 3000 rpm for 60 sec. to produce an ~500-nm thick film. The chip was prebaked for 45 sec. at 80 °C. The film was exposed to Xe light (300 W) for 45 sec. through a contact mask with a Cr metalized pattern on quartz. The chip was post-baked for 45 sec. at 80 °C and developed in Microchem SU8 developer for ~5 min. with intermittent sonication for 20 sec (three times in the process).The chip was then washed with water/isopropanol for ~60 sec and hard baked at 140 °C for 2 hr.

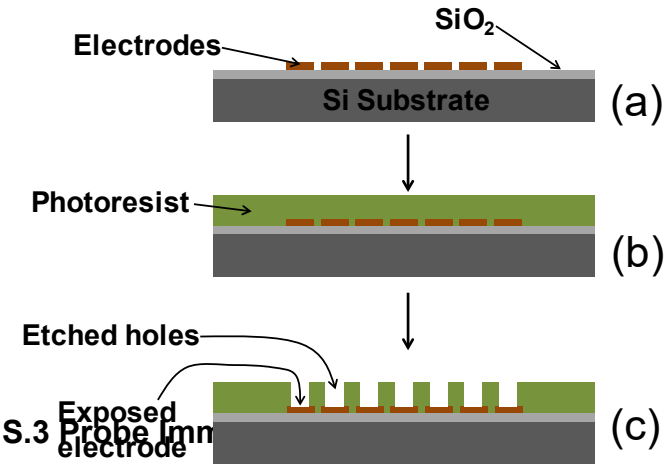

Figure S1: Cross-sectional view of the chip defined by A-A' in Fig. 1(a). Broadly, the photolithography had the following steps: (a) initial chip with electrodes; (b) after spin coating SU-8 photoresist; and (c) the chip after exposure to light and development to obtain a pattern of etched holes.

S.3 Probe Immobilization

Two types of probes were utilized in the study:

- P155: 5'-HS-$(CH_2)_6$-AAA- ACC CCT ATC ACG ATT AGC ATT AA 3'
- P21: 5'-HS-$(CH_2)_6$-AAA-TCA ACA TCA GTC TGA TAA GCT A-3'

The corresponding specific targets were:

- miR-155: 5' TTA ATG CTA ATC GTG ATA GGG GT 3'
- miR-21: 5' TAG CTT ATC AGA CTG ATG TTG A 3'

The immobilization on the spots was obtained by locally dispensing 5 µM solution of the probe in 1 M of phosphate buffer (PB) using an Arrayit® capillary pin (Fig. S2(a)). The capillary size of the pin was ~20 µm (Fig. S2(b), optical microscope image). The 5 nL solution dispensed on each spot was held by surface tension (Fig. S3). Each spot of the chip was exposed to the probe solution drop at 19 °C in a humidified chamber to avoid evaporation during the immobilization process for 2 hr. The chip was washed and the process repeated again to obtain higher immobilization density. All of the solutions and the washing were performed using RNAse-free water (Invitrogen).

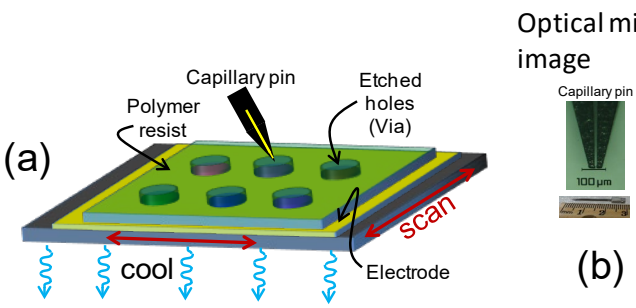

Figure S2: (a) The dispensing process was a typical spotting method with the chip on a motorized x-y stage, and the capillary pin (optical microscope image in (b)) was fixed. The solution was dispensed on various spots by moving the chip.

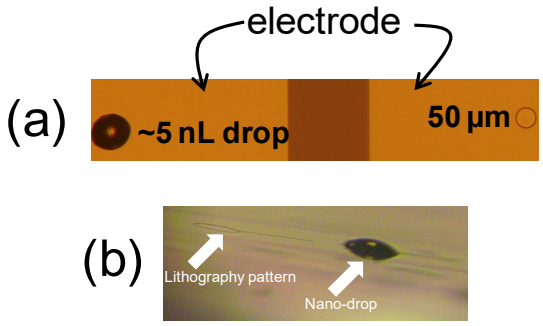

Figure S3: (a) One of the two etched 50-µm holes was covered with a solution of probe molecules. The dark region is the gap between the two electrodes. (b) A side view image of the drop confined by

S.4 MCH Filling Process

The MCH coating is one of the most critical aspects of the fabrication that decides the specificity and quality of measurement (see Section S.6 discussed later). The goal was to completely coat all of the exposed Au electrode surfaces after the the target binding step such that there was no signal on all of the three spots of the control electrode: the blank spot and the two spots with (immobilized) P155 and P21. The control electrode was not subjected to EFIB, thus the spots had no binding.

The MCH immobilization was performed in two steps. The chip was exposed to vapors from a 0.5 mL solution of 10 mM MCH in RNAse-free water (Invitrogen) at 37 °C for 10 hr. The process is called atomic layer deposition (ALD). The chip was dry with no condensation of water during ALD. After rinsing in autoclaved DI water, the chip was immersed in 1 mL solution of 10 mM MCH in 30% HPLC grade ethanol for 3 hours with vigorous shaking at 100 rpm in an incubator at 37 °C. The chip was subsequently rinsed and immersed in solution for differential reflectivity measurement. All of the solutions and washing /rinsing was performed in RNAse-free water (Invitrogen).

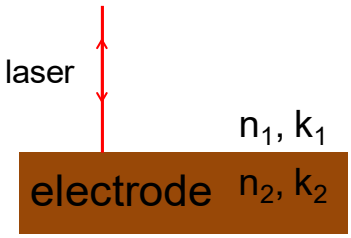

Figure S4: A schematic of the reflectivity kinematics defining the optical properties.

S.5 Oscillation of Reflected Light

Let (n_1,k_1) and (n_2,k_2) be the real and imaginary refractive index of the solution and electrode, respectively (Fig. S4), where $k_i = (\lambda/4\pi)\alpha_i$ (where α_i is the absorption coefficient of the material at wavelength, λ, of the incident light). In the most simplified case, it is assumed that there is no concentration gradient, thus n_1 is not a function of x. The assumption is not good; however, the analytical solution captures the principle of the measurement, i.e., the modulation of the reflectivity as average n_1 oscillates due to applied potential on the electrode. From Fresnel's law, the reflectivity, r, at normal incidence is,

$$r = \frac{(n_1 - n_2) - i(k_1 - k_2)}{(n_1 + n_2) - i(k_1 + k_2)} \quad (1)$$

Thus, the magnitude of reflectivity is,

$$|r|^2 = \left| \frac{\{(n_1^2 - n_2^2) - (k_1^2 - k_2^2)\}^2 + 4(n_1 k_1 - n_2 k_2)^2}{\{(n_1 + n_2)^2 + (k_1 + k_2)^2\}^2} \right|^2 \quad (2)$$

The refractive index is given by, $n_1 = n_w + (dn/dc)c$, where c is a concentration of various ions, dn/dc is the corresponding differential refractive index, and n_w is the refractive index of water. The details of the second term are not so critical, however, because the

polarizability of the anion is larger than the cation, the refractive index modulation of the former will dominate over the latter. For small modulation, $n_1 = n_w + \langle(dn/dc)c\rangle + (dn/dc)\delta c$, where δc is the perturbation around the equilibrium concentration profile due to the AC potential at frequency, ω. Generally, $\delta c = \delta c_o \cos(\omega t + \alpha)$, where δc_o is the amplitude of the ion oscillation and α is the phase difference between the applied potential and the ion oscillation. The phase difference is primarily due to viscosity effects. The details of the constants and the composition of the solution is not as critical. The important aspect is the application of the AC potential the concentration oscillates. Thus, the optical property of the solution is,

$$n_1 = \langle n_w + \frac{dn}{dc} c \rangle + B\cos(\omega t + \alpha) \quad (3)$$

where the first term in <...> is a time-independent quantity that will change with x and is complex in the sense it depends on concentration profiles of various ionic species. B is modified amplitude that includes δc_o and the differential refractive index. As the interest is to measure change in B as a function of applied ramp potential, E, the chemical details of B are not critical.

By substituting Equation (3) in (1) and linearizing with only first order terms, i.e., no higher order harmonics, 2ω, 3ω, and so on, the AC component of the reflectivity is,

$$R = K + Q\delta c_o \quad (4)$$

where K and Q are based on time-independent (i.e., equilibrium) optical properties of the solution and the electrode. Importantly, the differential reflectivity has a baseline (i.e., K) signal. The assumption of the linearity of the system is experimentally justified because the higher harmonics are over three orders of magnitude lower.

The principle is that at redox, due to discharge in the interfacial layer caused by electron exchange, the field penetration increases. As a result δc_o increases during redox current. Thus, from Equation (4), the potential, E, where R is maximum, will coincide with where the current due to oxidation and reduction reaction is highest.

The typical oscillation of the amplitude of reflectivity (R) at the detector (see Fig. 1(c)) as a function of periodic applied bias (E) on the WE with respect to the solution showed good periodicity with respect to E cycles (Fig. S5). A small portion of the scan is shown in Fig. 1(d).

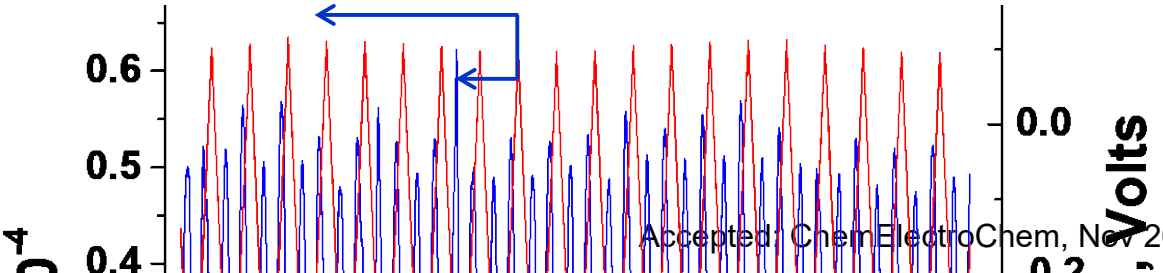

Figure S5: Typical scan of R as a function of t due to applied periodic potential E(t).

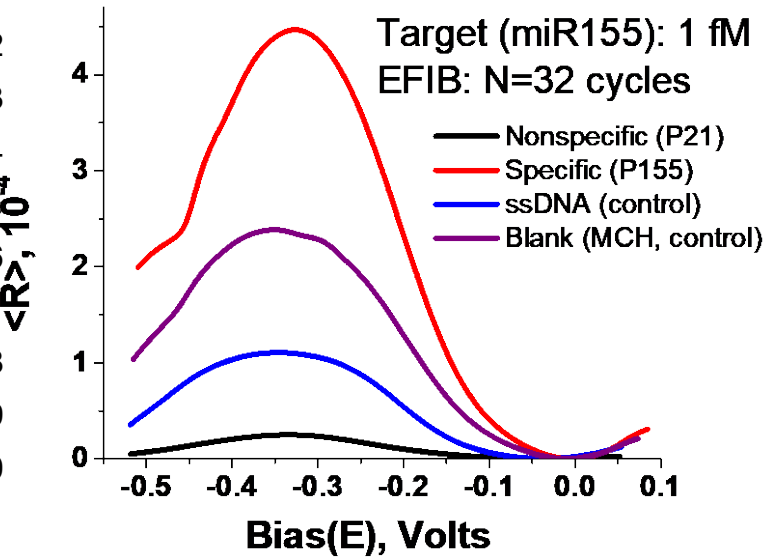

Figure S6: (a) Differential reflectivity from four spots when the MCH filling was not complete. The control (blank) shows complete MCH filling.

S.6 Effect of Incomplete MCH Coverage

Every chip was tested for quality of MCH coverage by measuring the signal on the three spots on the control electrode that were not subjected to EREB potential. The internal verification was critical to the quality of the data. The differential reflectivity measurement performed on the three sets of spots on the two control electrodes was blank (Au electrode coated with MCH); the spot with P155 was filled with MCH (ssDNA); and the

spot with P21 was filled with MCH (similar to ssDNA). In a chip with poor coverage, the blank and ssDNA show a peak due to MB redox due to pinholes (Fig. S6). As a result, the signal from a nonspecific spot was also positive indicating the specificity was not 100% (Fig. S6). Interestingly, the signal from a specific spot (i.e., spot with immobilized P155) was over threefold higher compared to the signal if the specificity was 100% (Fig. 2(a)) due to redox through the pinholes in the MCH monolayer. Such a chip was rejected for the study. The analysis on the control was performed for every chip prior to making the measurements on the five larger electrodes. A signal on the control spots will lead to poor specificity, and the specific signal would erroneously be considered over 3-fold higher. The spots with P155 and P21 probes on the control electrode showing no redox indicated that the signal was zero, if no binding occurred (i.e., ssDNA in Fig. 1(e)). Thus, the R_{max} reported here is an absolute measurement of the amount of specific binding. MCH deposition was after EREB.

S.7 Mixture Analysis

A binary miRNA mixture was studied where the concentration of the nonspecific target, miR21, was 10^3-fold larger. The effect of background miR21 showed that the signal for specific binding of miR155 was unchanged (Fig. S8). On the same chip with EFIB at N = 20, 28, and 32 (Fig. S8, inset), for the pure miR155 target (first bar for each N), the R_{max} on the P21 spot was zero (hatched bar), indicating 100% specificity, while R_{max} on the P155 spot (solid bar) was consistent with the calibration in Fig. 2(b). For each N, the signal for miR155 on the P155 spot (solid bar) was constant irrespective of the amount of miR21, indicating no interference from the latter. The signal for the 1 pM miR21 target on the P21 spot (third hatch bar for each N) was constant for all N, indicating saturation, as expected from Fig. 2(b).

For mixture analysis, a synthetic nonspecific probe sequence that did not match any of the known homo sapiens (hsa) mRNA sequences was used for the study. The sequence of the nonspecific probe was:

5’ ThioMC6-D/ GCA ATA ATG CTC TTT TTC AT 3’

The sequences of the five background miRNA used for Fig. 3(a) were:

miR 145: 5’ GTCCAGTTTTCCCAGGAATCCCT 3’

miR 29a: 5’ ACTGATTTTCTTTTGGTGTTCAG 3’

miR 630: 5’ AGTATTCTGTACCAGGGAAGGT 3’

miR 34a: 5’ TGGCAGTGTCTTAGATGGTTGT 3’

miR 16-1: 5’ TAGCAGCACGTAAAATATTGGCG 3’

Targets, miR155 (1 fM) and 21 (10 fM), were measured simultaneously in a background of these five miRNA each with a concentration of 1 pM.

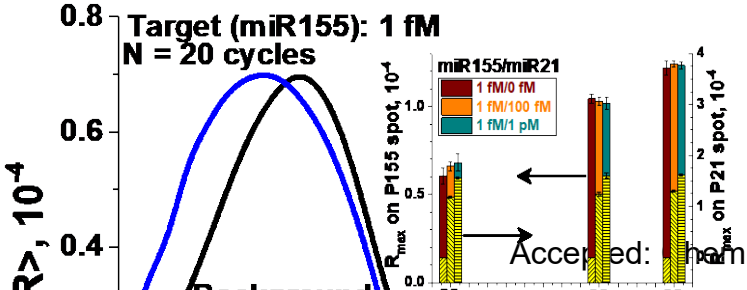

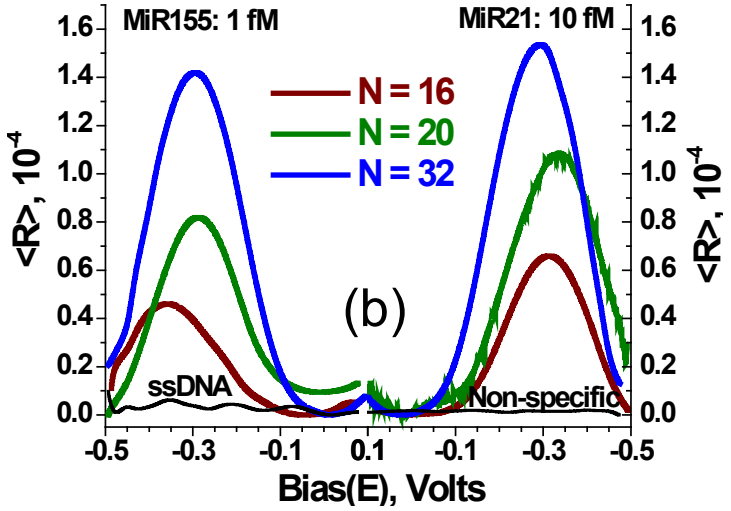

Figure S7: (a) Effect of background miR21 on <R> as a function of E on the same chip for specific binding to P155 and controls. Inset: A histogram of R_{max} for three chips measuring specific binding of a mixture to P155 and P21 spots. For each chip, EFIB was performed at three N each. The R_{max} data for miR155 and mi21 targets were each averaged over 15 and 6 points, respectively. (b) Typical <R> as function of E on the same chip for specific binding to P155 and P21 spots and the controls.

S.8 QPCR and SEED Analysis of miR39a for C. Elegans

The standard curve was obtained by making solutions of known amount of synthetic ssRNA of *C. elegans* miR39a (IDT, Inc., USA) target in sterile DNase/RNase-free water (Invitrogen, USA). SYBR Green method (Clontech Lab., Inc) was adopted to perform the cDNA synthesis and qPCR measurements on the qPCR machine (QuantStudio 3 RT-PCR, ABI, USA). In brief, 3.75 µL of a standard solution with known concentration was added to reverse transcriptase buffer and enzyme (the final reaction volume was 10 µL). The reaction was allowed to incubate at 37 ^{O}C for one hour, followed by denaturation of the RT enzyme at 85 ^{O}C for five minutes. The synthesized cDNA was diluted by 10-fold. A 0.8 µL portion was added to the master stock (SYBR Advantage Premix, ROX, miRNA-

specific 5' and 3' primers) resulting in the final volume of 10 µL. Melting curves on qPCR products were also generated to confirm specificity of the amplification. After qPCR, the data was analyzed while setting the threshold fluorescence to 0.059 arbitrary units. The mean values of CT were plotted as a function number of copies provided for reverse transcription to synthesize the cDNA (Fig. S9). Thus, the CT value corresponds to the number of miR39a mixed in the 3.75 µL solution. The standard curve was fit to the linear region of the semi-log plot.

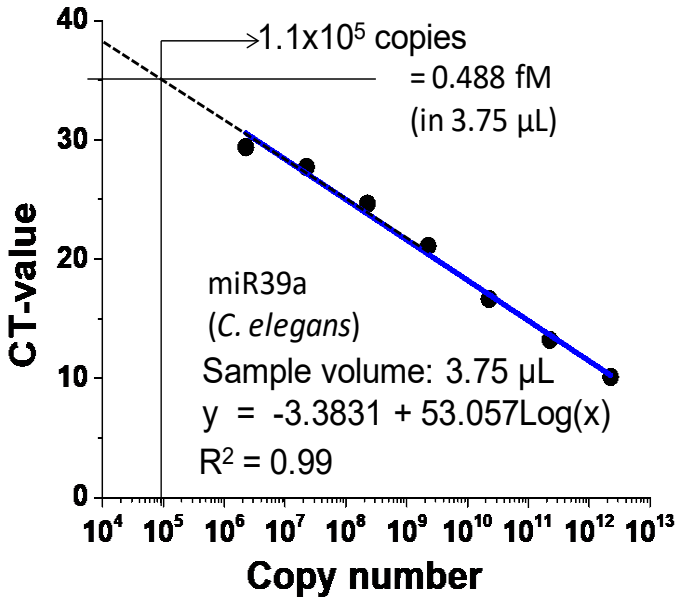

Figure S8: Standard curve of miR39a. The copy number is number of targer miRNA sequences in the RT-mix for cDNA conversion. Below 10^6 number of copies the CT valu is too low for reliability and the curve becomes non-linear.

To demonstrate the sensitivity and specificity for a complex biological sample, about ~14 µL of total RNA was extracted from ~200 µL of plasma from a healthy human subjects using a standard kit (RNeasy plus kit from Qiagen). The sample was reconstituted in 300 µL of PB buffer for EREB and spiked with synthetic miR39a of *C. elegans* at concentrations ranging from 0.01 to 10^3 fM. No miR39a is present in the human plasma sample. As the A-tail ligation, cDNA conversion and qPCR steps are avoided, direct binding of the miRNA to ssDNA probe is performed at 4 °C. For ssRNA (i.e., miRNA) as a target at low temperature, the EREB conditions are optimized to -0.4V to 0.5 V. R_{max} increases monotonically as the concentration of spiked miR39a increases, however, the signal is typically twofold larger than for ssDNA targets in Fig. 3(b). The signals from plasma (y-axis) and pure (x-axis) miR39a are literally identical along the 45° line (Fig. 3(b), inset).

Further to demonstrate multiplexing, we detect the presence of four circulating miRNAs (155, 21, 630 and 34a) in plasma and compare SEED results with QPCR. To precisely determine the accuracy of SEED signal conversion to the miRNA copies, we estimated <Rmax> based relative fold change for different miRNA in the normal and colorectal-cancer patient plasma samples, and compared with the gold standard PCR. The known amount of miR-39a (C. elegance miR control) was spiked in eluted RNA solution to the final concentration of 1 pM. Aliquot of the spiked RNA from the same RNA samples was

used to perform SEED and PCR so that both procedures start with the same solution to avoid any statistical inconsistencies.

We calculated the relative fold change of miRNA to 39a using the following equations:

a) Relative fold change using PCR $\sim 2^{\Delta Ct} \sim \frac{[miRNA]}{[39a]}$

b) Relative fold change using SEED $\sim 2^{log_2^{10}(\Delta R_{max})} \sim \frac{[miRNA]}{[39a]}$

where, [...] is molar concentration, which is equivalent to copy number.

Table: Comparative analysis of SEED and PCR based relative fold changes in multiple miRNAs of the normal and colorectal cancer patient plasma.

S.No.	Sequence	SEED		PCR		SEED/PCR
		R_{max}	Fold change relative to miR-39a	Ct values	Fold change relative to miR-39a	
a) Normal Plasma						
1.	miR-21	3.14 ± 0.26	14.76 ± 1.71	22.03 ± 0.48	13.61 ± 0.56	1.09 ± 0.14
2.	miR-34a	2.13 ± 0.33	0.69 ± 0.12	25.29 ± 0.28	1.41 ± 0.05	0.49 ± 0.09
3.	miR-155	0.88 ± 0.19	0.02 ± 0.003	29.66 ± 0.32	0.07 ± 0.003	0.22 ± 0.05
4.	miR-630	0.76 ± 0.23	0.01 ± 0.003	31.71 ± 0.13	0.02 ± 0.001	0.63 ± 0.20
b) Patient Plasma						
1.	miR-21	3.77 ± 0.26	99.72 ± 11.20	19.07 ± 0.75	105.64 ± 4.96	0.94 ± 0.12
2.	miR-34a	3.16 ± 0.35	15.80 ± 2.22	23.16 ± 0.45	6.20 ± 0.19	2.55 ± 0.37
3.	miR-155	0.92 ± 0.19	0.02 ± 0.003	30.28 ± 0.91	0.04 ± 0.002	0.38 ± 0.09
4.	miR-630	1.24 ± 0.25	0.04 ± 0.009	29.71 ± 0.46	0.07 ± 0.002	0.67 ± 0.14

References

1. A. J. Bard and L. R. Faulkner, *Electrochemical Methods: fundamentals and Applications* (J. Wiley & Sons, New York, 2001).
2. S. W. Lee, J. Lopez, and R. F. Saraf, Electroanalysis **25**, 1557-1566 (2013).
3. I. Y. Wong and N. A. Melosh, Nano Letters **9**, 3521-3526 (2009).
4. S. W. Lee, J. Lopez, and R. F. Saraf, Biosensors & Bioelectronics **47**, 408-414 (2013).
5. Z. L. Pei *et al.*, Oncotarget **8**, 22616-22624 (2017).
6. J. Tymoczko, et al. ACS Applied Materials & Interfaces **6**, 21851-21858 (2014).